Wideband Microwave Phase Noise Analyzer Based on an All-Optical Microwave I/Q Mixer

Jingzhan Shi, Fangzheng Zhang, *Member, IEEE*, De Ben, and Shilong Pan, *Senior Member, IEEE, Senior Member, OSA*

***Abstract*—Digital phase demodulation can greatly simplify the calibration of microwave phase noise analyzers (PNAs) based on frequency discriminators, and avoid the use of feedback loops, but the required microwave in-phase and quadrature (I/Q) mixer always has a small operational bandwidth, leading to a limited phase noise measurement frequency range. In this paper, a novel photonic microwave PNA based on digital phase demodulation is proposed and investigated, using an all-optical microwave I/Q mixer that consists of a Mach–Zehnder modulator, a polarization modulator and two polarizers. Different from conventional electrical I/Q mixers, which rely on electrical hybrids to introduce a 90-degree phase difference between the I and Q channels, the all-optical microwave I/Q mixer achieves the 90-degree phase difference by properly setting the polarizers, ensuring a broad operational bandwidth. The major problems associated with the use of the optical mixer in the PNA, i.e., DC interference and I/Q mismatch, are solved by tuning a variable delay-line together with post signal processing. In addition, to improve the phase noise measurement sensitivity, the time delay required in the frequency discriminator is implemented by a span of low-loss fiber. Experimental results show that the I/Q mixer can maintain a good performance within a frequency range from 5 to 40 GHz, and the proposed PNA has a high sensitivity (<-100 dBc/Hz@1 kHz and <-130 dBc/Hz@10 kHz).**

***Index Terms*—Phase noise, I/Q mixer, frequency discriminator, microwave photonics.**

I. Introduction

PHASE noise is an important parameter for evaluating the short-term frequency stability of a single-frequency signal source [1]. Microwave signal sources having a low phase noise and a large frequency tuning range are highly demanded in modern electronic systems such as radar, communication, and measurement systems [2]–[4]. The development of ultra-low phase noise microwave signal sources has put forward urgent requirements for high-sensitivity phase noise analysis of broadband-tunable microwave signal sources. Among the methods developed for phase noise analysis [5]–[7], phase noise measurement using a delay-line based frequency discriminator does not need a high-quality reference source, which can potentially achieve a larger measurement bandwidth and a better phase noise measurement sensitivity [8]. In the delay-line based frequency discriminator, as shown in Fig. 1(a), the signal under test (SUT) is first split into two branches, delayed in one branch by a certain time and then mixed in a frequency mixer with the one in the other branch. After a low-pass filter, phase noise of the SUT can be extracted. The phase noise measurement sensitivity is mainly determined by the amount of time delay. Since electrical delay lines are always bulky and lossy, optical delay lines realized by low-loss optical fiber can be applied to provide a much larger amount of time delay [9]–[16]. To enlarge the operational bandwidth which is mainly limited by the electrical components, microwave photonic phase shifters and mixers were also adopted to replace their electrical counterparts [12]–[15]. However, for any kind of frequency mixers, when converting the phase difference between the two input signals into a voltage signal, the conversion coefficient is dependent on the input power, which would introduce amplitude noise in the phase noise measurement. To ensure the measurement accuracy, the coefficient needs to be determined by a calibra-

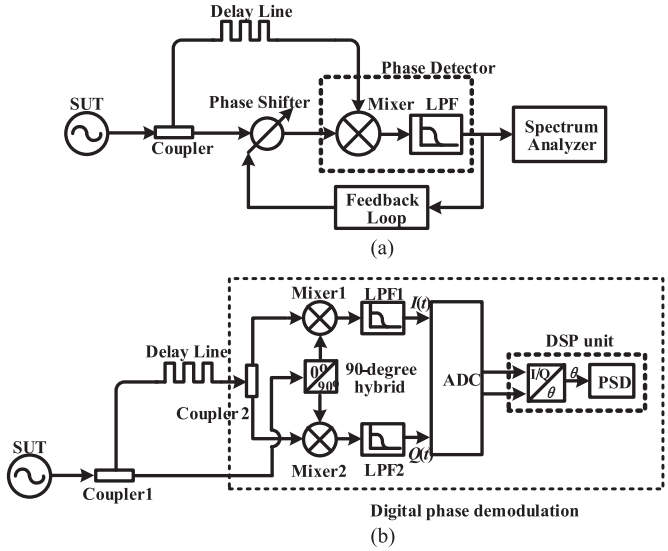

Fig. 1. (a) Schematic diagram of the delay-line based frequency discriminator system for phase noise measurement. SUT: signal under test. LPF: low pass filter. (b) Schematic diagram of the phase noise measurement system using digital phase demodulation. ADC: analog-to-digital converter; DSP: digital signal processing.

Manuscript received January 24, 2018; revised May 18, 2018; accepted May 24, 2018. Date of publication May 29, 2018; date of current version August 30, 2018. This work was supported in part by the NSFC program under Grant 61527820, in part by the Postgraduate Research and Practice Innovation Program of Jiangsu Province under Grant KYCX17_0289, and in part by the Fundamental Research Funds for the Central Universities under Grant NS2018028. *(Corresponding authors: Fangzheng Zhang; Shilong Pan.)*

The authors are with the Key Laboratory of Radar Imaging and Microwave Photonics, Ministry of Education, Nanjing University of Aeronautics and Astronautics, Nanjing 210016, China (e-mail: shijz@nuaa.edu.cn; zhangfangzheng@nuaa.edu.cn; bende01@sohu.com; pans@nuaa.edu.cn).

Color versions of one or more of the figures in this paper are available online at http://ieeexplore.ieee.org.

Digital Object Identifier 10.1109/JLT.2018.2841871

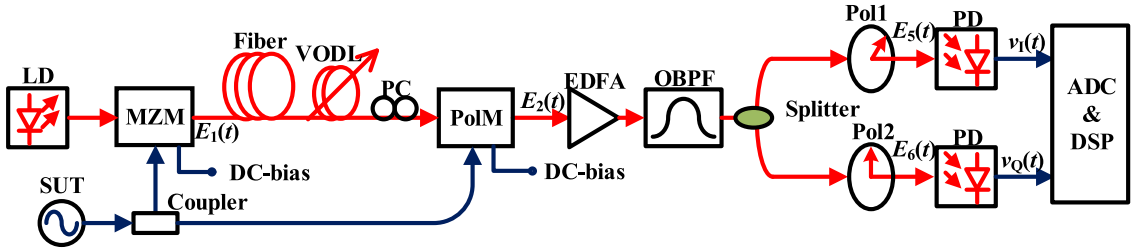

Fig. 2. Schematic diagram of the proposed PNA. LD: laser diode; MZM: Mach–Zehnder modulator; VODL: variable optical delay-line; PC: polarization controller; PolM: polarization modulator; EDFA: erbium-doped fiber amplifier; OBPF: optical bandpass filter; Pol: polarizer; PD: photodetector.

tion process using a signal source with known phase noise or a phase-modulated signal source. The amplitude and frequency of the signal source for calibration should be the same as those of the SUT, making the calibration extremely complicated. Besides, a phase shifter is required in one of the branches to keep a quadrature phase difference between the two input signals to the mixer, which ensures that the phase detector (i.e., the mixer and the low-pass filter) operates at a linear transmission point. The linear operational point is important to the phase noise measurement, at which the phase detector has the maximum phase-to-voltage and minimum amplitude-to-voltage conversion coefficients. Since the length of the optical fiber is usually dependent on temperature and environment vibration, in practice a feedback loop should be applied to automatically adjust the phase shifter. However, the use of the feedback loop not only complicates the system, but also suppresses the phase noise of the SUT within the bandwidth of the feedback loop because the phase noise to be measured is essentially a kind of phase drift.

To overcome the problems associated with the phase detector and the feedback loop, digital phase demodulation technique was proposed [17]–[20], which applies in-phase and quadrature (I/Q) frequency mixing to obtain the I and Q components of the downconverted signal, as shown in Fig. 1(b). With a certain algorithm, the phase noise can be calculated without introducing 90-degree phase difference between the delayed signal and the LO signal. As a result, the use of phase shifters and feedback loops is avoided. To increase the measurement sensitivity, previously, we established a microwave phase noise analyzer (PNA) based on an optical delay line and digital phase demodulation [19]. A phase noise measurement sensitivity of -134 dBc/Hz@10 kHz was demonstrated for a carrier frequency of 10 GHz. We also demonstrated that using a photonic-assisted I/Q mixer to replace the electrical mixer, a wide measurement bandwidth can be achieved [20]. However, an electrical 90-degree hybrid is required in the photonic-assisted I/Q mixer, which always has a limited bandwidth and uneven magnitude and phase responses. In addition, the photonic-assisted I/Q mixer would result in DC-interference problem in the PNA. To solve this problem, a two-step measurement was applied [20], with one measurement performed using the 90-degree hybrid and the other implemented using a 180-degree hybrid, making the measurement process sophisticated. Besides, [20] has ignored the problems of amplitude and phase mismatch between the I and Q channels, which may lead to considerable measurement error.

In this paper, a novel wideband PNA based on an all-optical microwave I/Q mixer and an optical delay line is proposed and experimentally investigated. Photonic-assisted microwave I/Q mixers have been demonstrated to have very wide operational bandwidth [21]–[23]. The I/Q mixer used in the proposed PNA is realized without any electrical hybrid, enabling a measurement bandwidth that only limited by the bandwidth of the electro-optical devices. Besides, we propose a method to solve the DC-interference and the I/Q-mismatch problems by simply tuning an extra variable optical delay line (VODL) followed by post signal processing. This paper is organized as follows. In Section II, the principle of the proposed PNA is described and the method to solve the DC-interference and I/Q-mismatch problems is proposed. In Section III, experimental investigation of the proposed PNA is carried out. Performance of the I/Q mixer, phase noise measurement accuracy, sensitivity, and measurement bandwidth are investigated. Section IV gives the conclusion.

II. Principle

Fig. 2 shows the schematic diagram of the proposed PNA based on an all-optical microwave I/Q mixer, which is realized by a zero-chirp Mach-Zehnder modulator (MZM), a polarization modulator (PolM) and two polarizers. A lightwave with a frequency of f_c generated by a laser diode (LD) is injected into the MZM biased at the quadrature point. The MZM is driven by the signal under test (SUT). Assume the SUT is expressed as $\cos[2\pi f_0 t + \varphi(t)]$, where f_0 and $\varphi(t)$ are the carrier frequency and phase fluctuation of the SUT, the optical field at the output of the MZM is given by

$$\begin{aligned} E_1(t) &\propto \cos\left\{\alpha\cos[2\pi f_0 t + \varphi(t)] + \frac{\pi}{4}\right\} e^{j\left(2\pi f_c t + \frac{\pi}{4}\right)} \\ &\approx \frac{\sqrt{2}}{2} J_0(\alpha) e^{j\left(2\pi f_c t + \frac{\pi}{4}\right)} \\ &\quad - \frac{\sqrt{2}}{2} J_1(\alpha)\left[e^{j2\pi(f_c - f_0)t - j\varphi(t) + j\frac{\pi}{4}}\right. \\ &\quad \left. + \; e^{j2\pi(f_c + f_0)t + j\varphi(t) + j\frac{\pi}{4}}\right] \end{aligned} \tag{1}$$

where α is the modulation index of the MZM. The output signal from the MZM is then sent to the PolM driven again by the SUT via a span of fiber and a VODL. The polarization direction of the incident light is oriented at an angle of 45° to one principal axis of the PolM. The PolM is a special phase modulator that can support both Transverse Electric (TE) and Transverse Magnetic

(TM) fields with opposite phase modulation indices [24]. The optical field after the PolM is written as

$$\begin{bmatrix} E_{\mathrm{x}}(t) \\ E_{\mathrm{y}}(t) \end{bmatrix} \propto \begin{Bmatrix} E_1(t-\tau_0-\tau_{\mathrm{v}})e^{j\beta\cos[2\pi f_0 t+\varphi(t)]+j\varphi} \\ E_1(t-\tau_0-\tau_{\mathrm{v}})e^{-j\beta\cos[2\pi f_0 t+\varphi(t)]} \end{Bmatrix} \quad (2)$$

where τ_0 and τ_{v} are the time delays introduced by the fiber and the VODL ($\tau_0 >> \tau_{\mathrm{v}}$), respectively, β is the phase modulation index of the PolM, and φ is the phase difference between E_{x} and E_{y}, which is adjusted to 90° by the DC-bias of the PolM. The output of the PolM is amplified and transmitted through an optical bandpass filter (OBPF), and then split into two branches, with each branch incorporating with a polarizer. Since the OBPF and polarizers are linear and passive devices, for simplicity we switch their orders in the following analysis.

Mathematically, when the PolM is followed by a polarizer of which the polarization direction has an angle of γ to one of the principal axes of the PolM, the optical field at the output of the polarizer is expressed as

$$E_2(t) \propto \cos\gamma \cdot E_{\mathrm{x}}(t) + \sin\gamma \cdot E_{\mathrm{y}}(t) \quad (3)$$

In the upper branch, γ is adjusted to 45°, so (3) can be rewritten as

$$\begin{aligned} E_3(t) &\propto \frac{\sqrt{2}}{2}E_1(t-\tau_0-\tau_{\mathrm{v}})e^{j\frac{\pi}{4}} \\ &\cdot \left\{e^{j\left[\beta\cos[2\pi f_0 t+\varphi(t)]+\frac{\pi}{4}\right]} + e^{-j\left[\beta\cos[2\pi f_0 t+\varphi(t)]+\frac{\pi}{4}\right]}\right\} \\ &= \sqrt{2}E_1(t-\tau_0-\tau_{\mathrm{v}})e^{j\frac{\pi}{4}} \\ &\cdot \cos\left\{\beta\cos[2\pi f_0 t+\varphi(t)]+\frac{\pi}{4}\right\} \end{aligned} \quad (4)$$

As can be seen, the PolM together with Pol1 functions as a zero-chirp MZM biased at the quadrature point. When γ is set to 90°, the PolM in combination with Pol2 functions as a phase modulator (PM), i.e.,

$$E_4(t) = E_{\mathrm{y}}(t) \propto E_1(t-\tau_0-\tau_{\mathrm{v}})e^{-j\beta\cos[2\pi f_0 t+\varphi(t)]} \quad (5)$$

The OBPF is used to select the -1st-order sideband of the modulated signal, so only the -1st-order sidebands in (4) and (5) are left. We obtain

$$\begin{aligned} E_5(t) &\propto -\frac{\sqrt{2}}{2}J_1(\alpha)J_0(\beta)e^{j\left[2\pi(f_c-f_0)(t-\tau_0-\tau_{\mathrm{v}})-\varphi(t-\tau_0-\tau_{\mathrm{v}})+\frac{\pi}{2}\right]} \\ &- \frac{\sqrt{2}}{2}J_0(\alpha)J_1(\beta) \\ &\times e^{j\left[2\pi(f_c-f_0)(t-\tau_0-\tau_{\mathrm{v}})-2\pi f_0(\tau_0+\tau_{\mathrm{v}})-\varphi(t)+\frac{\pi}{2}\right]} \\ E_6(t) &\propto -\frac{\sqrt{2}}{2}J_1(\alpha)J_0(\beta)e^{j\left[2\pi(f_c-f_0)(t-\tau_0-\tau_{\mathrm{v}})-\varphi(t-\tau_0-\tau_{\mathrm{v}})+\frac{3\pi}{4}\right]} \\ &- \frac{\sqrt{2}}{2}J_0(\alpha)J_1(\beta) \\ &\times e^{j\left[2\pi(f_c-f_0)(t-\tau_0-\tau_{\mathrm{v}})-2\pi f_0(\tau_0+\tau_{\mathrm{v}})-\varphi(t)+\frac{\pi}{4}\right]} \end{aligned} \quad (6)$$

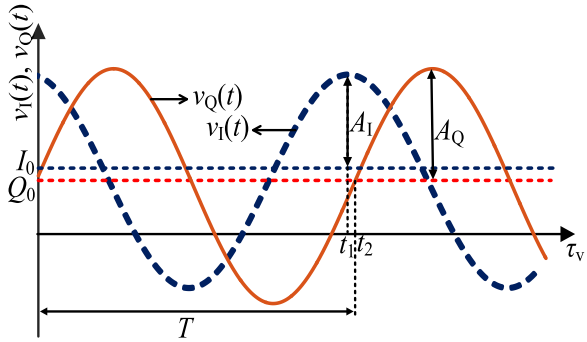

Fig. 3. $v_{\mathrm{I}}(t)$ and $v_{\mathrm{Q}}(t)$ as a function of τ_{v}.

Then, two photodetectors (PDs) are used for square-law detection in the upper and lower branches, respectively, which generates a pair of zero-intermediate-frequency voltages, given by

$$\begin{aligned} v_{\mathrm{I}}(t) &\propto R_1 Z_{\mathrm{L}}\|E_5(t)\|^2 = I_0 + I(t) \\ v_{\mathrm{Q}}(t) &\propto R_2 Z_{\mathrm{L}}\|E_6(t)\|^2 = Q_0 + Q(t) \end{aligned} \quad (7)$$

where R_1 and R_2 are the responsivities of the two PDs, respectively, Z_{L} is the input impendence, and

$$\begin{aligned} I_0 &= \frac{1}{2}R_1 Z_{\mathrm{L}}\left[J_1^2(\alpha)J_0^2(\beta) + J_0^2(\alpha)J_1^2(\beta)\right] \\ Q_0 &= \frac{1}{2}R_2 Z_{\mathrm{L}}\left[J_1^2(\alpha)J_0^2(\beta) + J_0^2(\alpha)J_1^2(\beta)\right] \\ I(t) &= -R_1 Z_{\mathrm{L}}J_1(\alpha)J_0(\beta)J_0(\alpha)J_1(\beta)\cos\left[\psi(t)\right] \\ Q(t) &= -R_2 Z_{\mathrm{L}}J_1(\alpha)J_0(\beta)J_0(\alpha)J_1(\beta)\sin\left[\psi(t)+\delta\varphi\right] \end{aligned} \quad (8)$$

where $\psi(t) = 2\pi f_0(\tau_0+\tau_{\mathrm{v}}) + \varphi(t) - \varphi(t-\tau_0-\tau_{\mathrm{v}})$, and $\delta\varphi$ is the phase mismatch between $I(t)$ and $Q(t)$ due to the different path lengths of the two branches. There is also amplitude mismatch (denoted as $k_{\mathrm{R}=}\, R_2/R_1$) between $I(t)$ and $Q(t)$ due to the different responsivities of the PDs in the two branches. According to (7) and (8), the phase term $\psi(t)$ can be calculated by

$$\begin{aligned} \psi(t) &= \mathrm{atan}\left(\frac{Q(t)-k_{\mathrm{R}}I(t)\sin(\delta\varphi)}{k_{\mathrm{R}}I(t)\cos(\delta\varphi)}\right) \\ &= \mathrm{atan}\left(\frac{[v_{\mathrm{Q}}(t)-Q_0]-k_{\mathrm{R}}[v_{\mathrm{I}}(t)-I_0]\sin(\delta\varphi)}{k_{\mathrm{R}}[v_{\mathrm{I}}(t)-I_0]\cos(\delta\varphi)}\right) \end{aligned} \quad (9)$$

As can be seen from (9), in order to figure out $\psi(t)$ based on the digitalized voltages $v_{\mathrm{I}}(t)$ and $v_{\mathrm{Q}}(t)$, the values of I_0, Q_0, k_{R}, and $\delta\varphi$ should be known. To do so, we slowly increase or decrease the time delay τ_{v} introduced by the VODL with a constant rate. Since the variation of τ_{v} only affects $I(t)$ and $Q(t)$ while maintain I_0 and Q_0 unchanged, as can be seen from (8), we can obtain I_0 and Q_0 by recording $v_{\mathrm{I}}(t)$ and $v_{\mathrm{Q}}(t)$ as a function of τ_{v}. The curves in Fig. 3 illustrates the voltages variations of $v_{\mathrm{I}}(t)$ and $v_{\mathrm{Q}}(t)$ when tuning the VODL, both complying with a sinusoidal function. With the two curves, the values of I_0, Q_0,

k_{R}, and $\delta\varphi$ can be calculated through

$$I_0 = \frac{\max[v_{\mathrm{I}}(t)] + \min[v_{\mathrm{I}}(t)]}{2}$$

$$Q_0 = \frac{\max[v_{\mathrm{Q}}(t)] + \min[v_{\mathrm{Q}}(t)]}{2}$$

$$k_{\mathrm{R}} = \frac{A_{\mathrm{Q}}}{A_{\mathrm{I}}} = \frac{\max[v_{\mathrm{Q}}(t)] - \min[v_{\mathrm{Q}}(t)]}{\max[v_{\mathrm{I}}(t)] - \min[v_{\mathrm{I}}(t)]}$$

$$\delta\varphi = \frac{360^{\mathrm{o}} \times (t_1 - t_2)}{T} \tag{10}$$

where max[$v(t)$] and min[$v(t)$] are the maximum and the minimum values of $v(t)$, respectively, A_{Q} and A_{I} are the amplitudes of $v_{\mathrm{I}}(t)$ and $v_{\mathrm{Q}}(t)$, respectively, t_1 represents the time when $v_{\mathrm{I}}(t)$ reaches its maximum, t_2 is the closest time to t_1 when $v_{\mathrm{Q}}(t)$ equals to Q_0, and T is the period of $v_{\mathrm{I}}(t)$ or $v_{\mathrm{Q}}(t)$, which is related to the carrier frequency of SUT and the tuning speed of the VODL.

After the values of I_0, Q_0, k_{R}, and $\delta\varphi$ are calculated, we stop changing the time delay τ_{v} for the following phase noise measurement. During the phase noise measurement, $\psi(t)$ can be figured out according to (9). Then, the single-sided PSD of $\psi(t)$ can be written as

$$S_{\psi}(f) = (2\pi f_0)^2 S_{\tau 0}(f) + (2\pi f_0)^2 S_{\tau v}(f) + S_{\Delta\varphi}(f) \tag{11}$$

where $S_{\psi}(f)$, $S_{\tau 0}(f)$, $S_{\tau v}(f)$, $S_{\Delta\varphi}(f)$ are the single-sided PSD of $\psi(t)$, τ_0, τ_{v}, and $\varphi(t) - \varphi(t - \tau_0 - \tau_{\mathrm{v}})$, respectively.

Considering that τ_0 is a constant and τ_{v} is also a constant after we stop tuning the VODL, the first and the second components of $S_{\psi}(f)$ only make contributions to $S_{\psi}(f)$ at the offset frequency of 0, so we have

$$S_{\Delta\varphi}(f) = S_{\psi}(f), \quad f \neq 0 \tag{12}$$

According to [19], the relationship between the single-sided PSD of $\varphi(t) - \varphi(t - \tau_0 - \tau_{\mathrm{v}})$ and that of the phase fluctuation $\varphi(t)$ is

$$S_{\varphi}(f) = \frac{S_{\Delta\varphi}(f)}{4\sin^2[\pi f(\tau_0 + \tau_{\mathrm{v}})]} \approx \frac{S_{\Delta\varphi}(f)}{4\sin^2(\pi f \tau_0)} \tag{13}$$

where $S_{\varphi}(f)$ is the single-sided PSD of $\varphi(t)$. The time delay τ_{v} introduced by the VODL is ignored in (13) because it is far less than the time delay τ_0 introduced by the fiber.

Phase noise of the SUT, denoted by $L(f)$, is one-half of the single-sided PSD of the phase fluctuation $\varphi(t)$ [1], given by

$$L(f) = \frac{S_{\varphi}(f)}{2} = \frac{S_{\psi}(f)}{8\sin^2(\pi f \tau_0)}, \quad f \neq 0 \tag{14}$$

In (14), the phase noise values at the offset frequency of zero is not included. In most of the cases, the phase noise at zero is not of interest.

III. Experimental Results and Discussion

Based on the setup in Fig. 2, an experiment is carried out to investigate the performance of the proposed PNA. The photograph of the experiment system is shown in Fig. 4, and the parameters of the devices are listed in Table I. In the experiment,

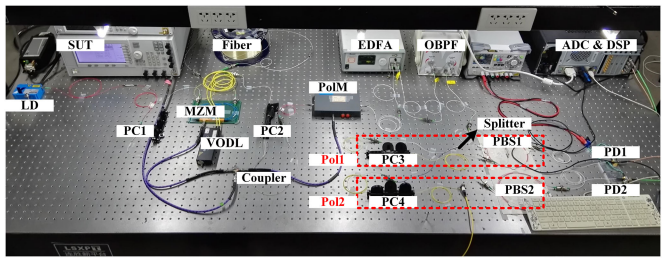

Fig. 4. Photograph of the experimental setup. PBS: polarization beam splitter.

TABLE I
Parameters of the Main Devices in the Experimental Setup

Device	Manufacturer, Version	Parameters
LD	TeraXion, PS-NLL-1550.52-080-000-A1	Wavelength: 1550.52 nm; Output Power: 19 dBm
MZM	EOSPACE, AX-0MVS-40-PSA-FSA	3-dB bandwidth: 40 GHz; Half-wave voltage: 8 V
Fiber	YOFC, TBF-I-VY-1B1.3	Length: 2-km SMF[a]
VODL	General Photonics, VDL-001-15-600-SM-FC/APC	Range of time delay: 0-600 ps
PolM	Versawave, PL-40G-3-1550-V-FC P-FCU	3-dB bandwidth: 40 GHz
EDFA	Amonics, AEDFA-35-B-FA	Gain: >35 dB (input power < -10 dBm)
OBPF	Yenista, XTM-50/S	Tuning range: 1450-1650 nm; Bandwidth: 50-950 pm; Edge roll-off: 500 dB/nm
PD1,2	Discovery Semiconductors, DSC50S	3-dB bandwidth: 12 GHz; Responsivity: 0.8 A/W@1550 nm
ADC	National Instruments, PXI-4462	Sampling frequency: 204.8 kHz; Number of channels: 4; Sampling resolution: 24 bit
Coupler	Malaysia	Frequency range: 0-50 GHz

[a]SMF: single-mode fiber.

a polarization controller (PC) followed by a polarization beam splitter (PBS) is used as a polarizer. The polarization angle of the equivalent polarizer can be tuned by adjusting the PC.

A. All-optical Microwave I/Q Mixer

Before phase noise measurement, performance of the all-optical microwave I/Q mixer is investigated. In the experiment, a 10.01-GHz signal generated by an analog signal generator (Agilent, E8257D-option 567) and a 10-GHz signal generated from another signal generator (Agilent, E8257D-option 540) are sent to the RF-port of the MZM and PolM, respectively. The -1$^{\mathrm{st}}$-order sidebands of the optical signal after the PolM is selected by an OBPF. Fig. 5(a) shows the response of the OBPF, and the optical spectra of the optical signals at the outputs of the MZM and the PolM and the signal after the OBPF, which are measured by an optical spectrum analyzer with a resolution of 20 pm (YOKOGAWA, AQ6370C). At the output of the two PDs, a pair of 10-MHz intermediate-frequency (IF) signals are

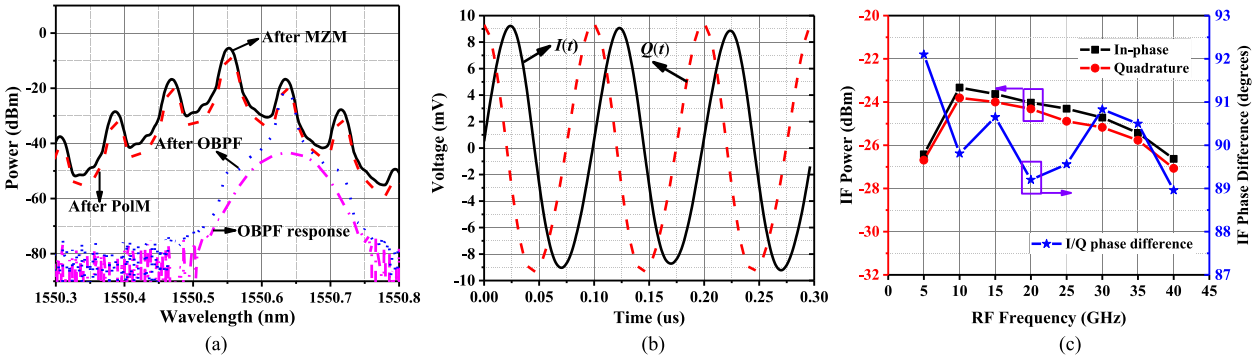

Fig. 5. (a) The response of the OBPF (dash-dotted curve), and the spectra of the optical signals at the outputs of the MZM (solid curve) and the PolM (dashed curve), and the spectrum of the lightwave after the OBPF (dotted curve), (b) the waveforms of the obtained 10-MHz IF signals, and (c) the powers of the IF signals and phase difference between them as a function of RF frequency.

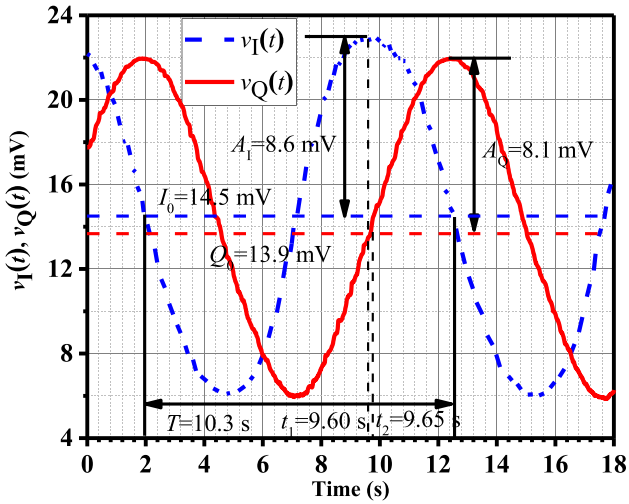

Fig. 6. A pair of digitalized tracks after the ADCs as the time delay τ_v changes with a constant rate.

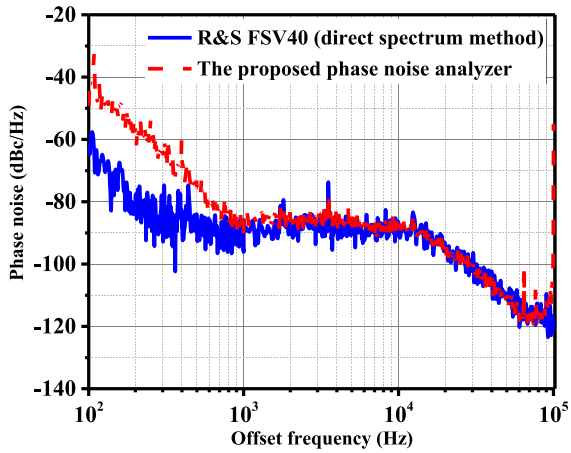

Fig. 7. Phase noise of a 10-GHz clock signal measured by R&S FSV40 (solid curve) and that measured by the proposed PNA (dashed curve).

obtained. To eliminate the DC components in the signals, a DC block is connected to each PD. A four-channel 32-GHz digital oscilloscope (Agilent, DSO-X 92504A) is used to record the waveforms of the two IF signals. As shown in Fig. 5(b), the two IF signals have almost equal amplitudes and a 90-degree phase difference, which indicates the proposed I/Q mixer is feasible.

Next, power balance and phase mismatch between the I and Q channels are measured as a function of the input RF frequency. In the measurement, frequency of the signal applied to the MZM is tuned from 5 to 40 GHz with a step of 5 GHz, and frequency of the signal driving the PolM is tuned accordingly to be 10 MHz lower such that the output IF signal has a fixed frequency. The measurement results are shown in Fig. 5(c). As can been seen, the proposed I/Q mixer is able to maintain a small power mismatch (<1 dB) and a good quadrature-phase difference (variation within 3°) between the I and Q channels, when the input RF signal changes in a very large frequency range from 5 to 40 GHz. For RF frequency from 10 to 40 GHz, the conversion gain decreases as the RF frequency increases, which is attributed to the frequency dependence of the electro-optic modulation responses of the MZM and the PolM. For RF frequency at 5 GHz, the mixer has a relatively low IF output power and a large phase mismatch, because the OBPF has a limited roll-off factor.

B. Phase Noise Measurement Accuracy

In order to verify the measurement accuracy of the proposed PNA, the phase noise of a 10-GHz clock signal generated by a pulse pattern generator (Anritsu MP1763C) is measured. In the measurement, the time delay provided by the VODL is slowly adjusted with a constant speed. The obtained signals in the I and Q channels difference, $v_I(t)$ and $v_Q(t)$), are digitized by two ADCs, with the results shown in Fig. 6. Based on the results in Fig. 6, the values of I_0, Q_0, k_R, and $\delta\varphi$ can be calculated according to (10), i.e., $I_{0=}$ 14.5 mV, $Q_{0=}$ 13.9 mV, $k_R = 0.94$, and $\delta\varphi = -1.75°$. Then, the phase noise of the 10-GHz clock signal is obtained according to (9) and (14). The dashed curve in Fig. 7 shows the measurement result using the proposed phase noise analyzer. As a comparison, the phase noise of the same signal is also measured by a commercial signal source analyzer (R&S FSV40) [25], which is plotted as the solid line in Fig. 7. It can be seen that the measured result by the proposed PNA agrees well with that measured by FSV40, especially at offset frequencies

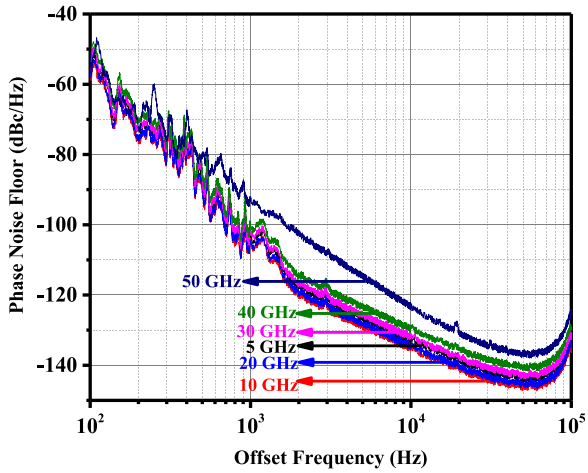

Fig. 8. Phase noise floor of the proposed PNA for different carrier frequencies.

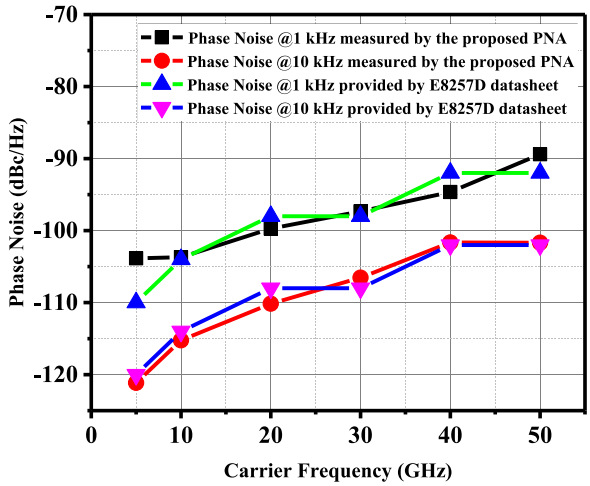

Fig. 9. Phase noise at offset frequencies of 1 and 10 kHz of signals having different carrier frequencies generated by E8257D measured by the proposed phase noise analyzer and those provided by the E8257D datasheet.

TABLE II
PHASE NOISE FLOOR AT OFFSET FREQUENCIES OF 1 AND 10 KHZ FOR DIFFERENT CARRIER FREQUENCIES

Carrier Frequency, GHz	Phase Noise Floor @1 kHz, dBc/Hz	Phase Noise Floor @10 kHz, dBc/Hz
5	-104	-133
10	-106	-136
20	-106	-135
30	-103	-132
40	-101	-130
50	-94	-124

larger than 1 kHz. At offset frequencies lower than 1 kHz, there is evident difference between the results, which is mainly caused by two factors. One factor is the conversion coefficient from the PSD of the phase term $\psi(t)$ to the phase noise $L(f)$. According to (14), the coefficient is $1/8\sin^2(\pi f\tau_0)$, which is infinite at offset frequencies of N/τ_0 ($N = 0, 1, 2, \ldots$). When $N = 0$ is considered, the measured phase noise at the offset frequencies near zero will be higher than the real value. The other factor is the length drift of the long optical fiber. As shown in (11), when the time delay τ_0 is not a constant, the PSD of the phase term $\psi(t)$ will not only contain the PSD of $\varphi(t) - \varphi(t - \tau_0 - \tau_v)$, but also contain the PSD of $2\pi f\tau_0$. The varying τ_0 only has influence on the measured result at low offset frequencies, because the drift of the time delay provided by the fiber is caused by the slowly varying temperature (typically <1 kHz) or vibration from the environment. It should be noted that it is a common problem for all frequency-discriminator-based PNA [17], [20].

C. Phase Noise Measurement Sensitivity

Phase noise measurement sensitivity is evaluated by phase noise floor, which refers to the minimum phase noise that can be measured by the PNA. As suggested in [20], the phase noise floor can be measured by replacing the fiber with an optical attenuator, which has the same insertion loss with the fiber. In order to measure the phase noise floor for different carrier frequencies, a wideband signal source (E8257D-option 567) is used to generate signals with carrier frequencies from 5 to 50 GHz. Fig. 8 shows the measured phase noise floors for different carrier frequencies. Table II lists the specific phase noise floor at the offset frequencies of 1 and 10 kHz, respectively. As can be seen, the phase noise floor of the proposed PNA is generally lower than -100 dBc/Hz at the 1-kHz offset frequency and lower than -130 dBc/Hz at the 10-kHz offset frequency within a large carrier-frequency range from 5 to 40 GHz, respectively. For 50-GHz carrier frequency, the phase noise floor is obviously degraded. In general, the phase noise floor is related to carrier frequency because the IF power of the proposed I/Q mixer are related to carrier frequency, as shown in Fig. 5(c), and according to [17], the phase noise floor increases with the decrease of IF power. The phase noise measurement sensitivity can be further improved through two methods. One method is to increase the time delay τ_0 by using a longer fiber. However, when the time delay is increased, the reliable offset frequency range for phase noise measurement will be reduced. The other method is to apply two-channel cross correlation. By averaging the cross spectrum of the phase terms $\psi(t)$ obtained from the two channels, the uncorrelated noise can be suppressed and the phase noise measurement sensitivity can be improved by up to 20 dB by averaging 10000 times [9].

D. Operational Bandwidth

Thanks to the use of broadband all-optical microwave I/Q mixer, the proposed PNA is able to operate in a large carrier-frequency range. In order to demonstrate this property, the phase noise of RF signals with 5-GHz, 10-GHz, 20-GHz, 30-GHz, 40-GHz, and 50-GHz carrier frequencies generated by the signal source (E8257D-option 567) are tested by the proposed PNA, without using a signal source with the same power and frequency as well as known phase noise for calibration. The measured phase noise at offset frequencies of 1 and 10 kHz are plotted in Fig. 9. As a comparison, the phase noises listed in the E8257D datasheet [26] is also plotted. As can be seen, the differences between the measured results and those provided by the E8257D datasheet are less than 3 dB except for the 6-dB difference at 1-kHz offset frequency for 5-GHz carrier frequency.

The large difference is because of the limited sensitivity of the proposed PNA at 5-GHz carrier frequency, as shown in Fig. 8.

IV. Conclusion

In this paper, we have proposed and demonstrated a wideband PNA based on an all-optical microwave I/Q mixer and an optical delay line, which shows advantages of large operational bandwidth, high sensitivity, and simple calibration. The proposed PNA can find application in characterization of high-frequency signal sources with ultra-low phase noise.

References

[1] *IEEE Standard Definitions of Physical Quantities for Fundamental Frequency and Time Metrology – Random Instabilities*, IEEE Standard 1139, 2008.

[2] L. P. Goetz and W. A. Skillman, "Master oscillator requirements for coherent radar sets," in *Proc. IEEE–NASA Symp. Short-Term Freq. Stability*, Greenbelt, MD, USA, 1964, pp. 19–27.

[3] R. L. Sydnor, "Short-term stability requirements for deep space tracking and communication systems," in *Proc. IEEE–NASA Symp. Short-Term Freq. Stability*, Greenbelt, MD, USA, 1964, pp. 43–50.

[4] J. J. Caldwell Jr., "Satellite range and tracking accuracy as a function of oscillator stability," in *Proc. IEEE–NASA Symp. Short-Term Freq. Stability*, Greenbelt, MD, USA, 1964, pp. 39–41.

[5] D. B. Leeson, "Oscillator phase noise: A 50-year review," *IEEE Trans. Ultrason. Ferroelectr. Freq. Control*, vol. 63, no. 8, pp. 1208–1225, Aug. 2016.

[6] U. L. Rohde, A. K. Poddar, and A. M. Apte, "Getting its measure: Oscillator phase noise measurement techniques and limitations," *IEEE Microw. Mag.*, vol. 14, no. 6, pp.73–86, Sep./Oct. 2013.

[7] M. Jankovic, "Phase noise in microwave oscillators and amplifiers," Ph.D. dissertation, Dept. Elect, Comput. Energy Eng, Facul. Grad. School Univ. Colorado, Boulder, CO, USA, 2010.

[8] C. Schiebold, "Theory and design of the delay line discriminator for phase noise measurements," *Microw. J.*, vol. 26, no. 12, pp. 103–112, Dec. 1983.

[9] S. L. Pan and J. P. Yao, "Photonics-based broadband microwave measurement," *J. Lightw. Technol.*, vol. 35, no. 16, pp. 3498–3513, Aug. 2017.

[10] E. Rubiola, E. Salik, S. Huang, N. Yu, and L. Maleki, "Photonic-delay technique for phase-noise measurement of microwave oscillators," *J. Opt. Soc. Amer. B*, vol. 22, no. 5, pp. 987–997, May 2005.

[11] P. Salzenstein *et al.*, "Realization of a phase noise measurement bench using cross correlation and double optical delay line," *Acta Phys. Pol. A*, vol. 112, no. 5, pp. 1107–1111, Sep. 2007.

[12] D. J. Zhu, F. Z. Zhang, P. Zhou, D. Zhu, and S. L. Pan, "Wideband phase noise measurement using a multifunctional microwave photonic processor," *IEEE Photon. Technol. Lett.*, vol. 26, no. 24, pp. 2434–2437, Dec. 2014.

[13] W. T. Wang, J. G. Liu, H. K. Mei, W. H. Sun, and N. H. Zhu, "Photonic-assisted wideband phase noise analyzer based on optoelectronic hybrid units," *J. Lightw. Technol.*, vol. 34, no. 14, pp. 3425–3431, Jul. 2016.

[14] D. J. Zhu, F. Z. Zhang, P. Zhou, and S. L. Pan, "Phase noise measurement of wideband microwave sources based on a microwave photonic frequency down-converter," *Opt. Lett.*, vol. 40, no. 7, pp. 1326–1329, Apr. 2015.

[15] F. Z. Zhang, D. J. Zhu, and S. L. Pan, "Photonic-assisted wideband phase noise measurement of microwave signal sources," *Electron. Lett.*, vol. 51, no. 16, pp. 1272–1274, Aug. 2015.

[16] N. Kuse and M. E. Fermann, "Electro-optic comb based real time ultra-high sensitivity phase noise measurement system for high frequency microwaves," *Sci. Rep.*, vol. 7, no. 1, pp. 2847–2854, Jun. 2017.

[17] S. O. Tatu, E. Moldovan, S. Affes, B. Boukari, K. Wu, and R. G. Bosisio, "Six-port interferometric technique for accurate W-band phase-noise measurements," *IEEE Trans. Microw. Theory Techn.*, vol. 56, no. 6, pp. 1372–1379, Jun. 2008.

[18] H. Gheidi and A. Banai, "Phase-noise measurement of microwave oscillators using phase-shifterless delay-line discriminator," *IEEE Trans. Microw. Theory Techn.*, vol. 58, no. 2, pp. 468–477, Feb. 2010.

[19] J. Z. Shi, F. Z. Zhang, and S. L. Pan, "High-sensitivity phase noise measurement of RF sources by photonic-delay line and digital phase demodulation," in *Proc. Int. Conf. Opt. Commun. Netw.*, Wuzhen, China, Aug. 2017, pp. 7–10.

[20] F. Z. Zhang, J. Z. Shi, and S. L. Pan, "Wideband microwave phase noise measurement based on photonic-assisted I/Q mixing and digital phase demodulation," *Opt. Exp.*, vol. 25, no. 19, pp. 22760–22768, Sep. 2017.

[21] P. Y. Li, X. H. Zou, W. Pan, and L. S. Yan, "Microwave photonic down-conversion with large image rejection ratio utilizing digital signal processing," in *Proc. Asia Commun. Photon. Conf.*, Wuhan, China, Nov. 2016, Paper ATh3H.3.

[22] Z. Z. Tang and S. L. Pan, "Image-reject mixer with large suppression of mixing spurs based on a photonic microwave phase shifter," *J. Lightw. Technol.*, vol. 34, no. 20, pp. 4729–4735, Oct. 2016.

[23] Y. S. Gao, A. J. Wen, Z. Y. Tu, W. Zhang, and L. Lin, "Simultaneously photonic frequency downconversion, multichannel phase shifting, and IQ demodulation for wideband microwave signals," *Opt. Lett.*, vol. 41, no. 19, pp. 4484–4487, Oct. 2016.

[24] S. L. Pan and J. P. Yao, "A frequency-doubling optoelectronic oscillator using a polarization modulator," *IEEE Photon. Technol. Lett.*, vol. 21, no. 13, pp. 929–931, Jul. 2009.

[25] *R&S FSV-K40 Phase Noise Measurement Application (Data Sheet) Version 02.00.* Munich, Germany: Rohde & Schwarz, 2014, p. 4.

[26] *E8257D PSG Microwave Analog Signal Generator Data Sheet*. California, USA: Keysight Technologies, 2016, p. 20.

Jingzhan Shi received the B.S. and M.S. degrees in electronic and information engineering from Nanjing University of Aeronautics and Astronautics (NUAA), Nanjing, China, in 2013 and 2016, respectively, where he is currently working toward the Ph.D. degree at the Key Laboratory of Radar Imaging and Microwave Photonics.

His current research interest is phase noise measurement of microwave signals.

Fangzheng Zhang (S'10–M'13) received the B.S. degree from Huazhong University of Science and Technology (HUST), Wuhan, China, in 2008, and the Ph.D. degree from Beijing University of Posts and Telecommunications (BUPT), Beijing, China, in 2013. He is currently with the College of Electronic and Information Engineering, Nanjing University of Aeronautics and Astronautics, as an associate professor.

His main research interests include microwave photonics, coherent optical communications and all-optical signal processing.

De Ben, biography not available at the time of publication.

Shilong Pan (S'06–M'09–SM'13) received the B.S. and Ph.D. degrees in electronics engineering from Tsinghua University, Beijing, China, in 2004 and 2008, respectively. From 2008 to 2010, he was a "Vision 2010" Postdoctoral Research Fellow in the Microwave Photonics Research Laboratory, University of Ottawa, Canada. He joined the College of Electronic and Information Engineering, Nanjing University of Aeronautics and Astronautics, China, in 2010, where he is currently a Full Professor and an Executive Director of the Key Laboratory of Radar Imaging and Microwave Photonics, the Ministry of Education.

His research has focused on microwave photonics, which includes optical generation and processing of microwave signals, analog photonic links, photonic microwave measurement, and integrated microwave photonics. He has authored or co-authored over 360 research papers, Including more than 190 papers in peer-reviewed journals and 170 papers in conference proceedings.

Prof. Pan is currently a Topical Editor of *Chinese Optics Letters*. He was selected to receive an OSA outstanding reviewer award in 2015 and a top reviewer for the IEEE/OSA Journal of Lightwave Technology in 2016. He served as a Chair of numerous international conferences and workshops, including the TPC Chair of IEEE ICOCN 2015, TPC Co-chair of IEEE International Topical Meeting on Microwave Photonics in 2017, TPC Chair of the high-speed and broadband wireless technologies subcommittee of the IEEE Radio Wireless Symposium in 2013, 2014, and 2016, TPC Chair of the Optical fiber sensors and microwave photonics subcommittee of the OECC in 2015, and Chair of the microwave photonics for broadband measurement workshop of the International Microwave Symposium in 2015.